Q. J. R. Meteorol. Soc. (2006), **132**, pp. 2853–2860 doi: 10.1256/qj.05.239

Synoptic-scale weather patterns during Alpine heavy rain events

By KLAUS P. HOINKA[1]*, CORNELIA SCHWIERZ[2] and OLIVIA MARTIUS[2]

[1]*Institut für Physik der Atmosphäre, DLR, Oberpfaffenhofen, Germany*
[2]*Institut für Atmosphäre und Klima, ETH, Zürich, Switzerland*

(Received 28 December 2005; revised 18 May 2006)

SUMMARY

Autumnal streamer-type elongated troughs are related to heavy precipitation observed at the southside of the European Alps. In order to study the development of this configuration, the typical structural evolution of the ambient flow in the event of heavy rain is investigated by lagged analyses. The precipitation amounts, both observations at the Alpine southside and from ERA40 forecasts by the ECMWF, are chosen as parameters to be correlated with atmospheric fields provided by the ERA40 data. Indeed, the resulting statistics indicate that the preferable position of elongated streamers is quasi-north–south aligned and extending southward over the Mediterranean Sea with its southern end located between the Pyrenees and northern Africa. A significant orographic impact on the streamer is revealed in the regression fields of the upper-level potential vorticity showing an indentation above the western Alps. The lower-tropospheric regression fields show a zonally elongated pressure signal due to the orographic influence. Up to two days in advance of heavy rain events a regressed meridional humidity flux occurs towards the south-western Alps, which at the event's peak time is found impinging upon the entire Alpine ridge. The regressed vertical velocity fields exhibit two maxima south of the Alps, a strong one at the western and a weaker one over the eastern Alps.

KEYWORDS: Alps flooding ERA40 PV-streamer

1. INTRODUCTION

Western Europe is a preferred region for the occurrence of narrow meridionally elongated troughs, which may extend equatorward from Britain towards the Iberian Peninsula (Holopainen and Rontu 1981). These elongated troughs are characterized by high values of potential vorticity (PV) and are therefore termed 'PV-streamer' (Appenzeller and Davies 1992). Among others, Massacand *et al.* (1998) pointed out that these upper-tropospheric troughs accompany events of heavy precipitation on the southern slopes of the Alps. In the last decades, various notable events occurred which exhibited the characteristic synoptic features of streamers combined with heavy precipitation at the Alpine southside, e.g. the 'Brig-event' on 23 September 1993 and the 'Piedmont-event' on 5 November 1994, both with a maximum rain rate of more than 220 mm per 24 h.

The knowledge of the streamer's impact on regional heavy precipitation is a necessary prerequesite for a successful numerical weather prediction (NWP). Numerical simulations were performed in order to understand this impact and its significance for NWP as outlined by various studies in special journal issues of international projects (Mesoscale Alpine Programme (MAP) (Bougeault *et al.* 2003); Heavy Precipitation in the Alpine Region (HERA) (Volkert 2000)). Coordinated experimental efforts, such as the MAP experiment, helped further to understand the streamer's evolution and its impact on the generation of flooding. The climatological relationship between heavy precipitation along the Alpine southside and upper-tropospheric PV-streamers over western Europe was investigated in a recent study by Martius *et al.* (2006, hereafter MZSD). They determined climatological statistics of streamers based on the ERA40 data (Simmons and Gibson 2000) provided by the European Centre for Medium-Range Weather Forecasts (ECMWF) and related them to observed precipitation data (Frei and Schär 1998). The resulting structure of the averaged upper-tropospheric PV field shows the typical PV-streamer spatial pattern known from various prominant events (Massacand *et al.* 1998): quasi-north–south aligned; extending southward over the Mediterranean Sea with its southern end located between the Pyrenees and northern Africa.

The study of MSZD showed also that the combination of a synoptic-scale PV-streamer associated with heavy rain above the Alps is not a rare event. For a 34-year (1966–99) period they determined about 4 days per year with heavy precipitation of more than 29 mm d^{-1} on the Alpine southside. The time series of rain rates used consists of area-mean values representative for southern Switzerland. On average about 3 days per year of the heavy precipitation subsample showed the presence of an upper-level streamer over western Central Europe, whereas the rest of this subsample contains days with other features, e.g. the

* Corresponding author: Institut für Physik der Atmosphäre, DLR, Postfach 1116, D-82230 Wessling, Germany.
e-mail: Klaus.Hoinka@dlr.de

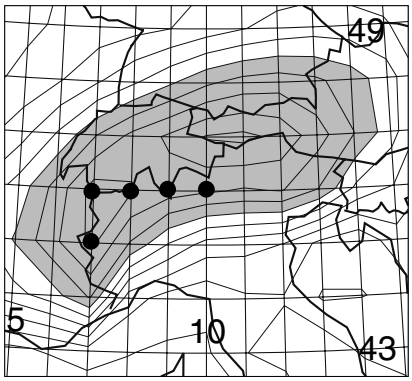

Figure 1. The Alps as represented in the ERA40 dataset. The increment of the isolines is 125 m. The shaded area shows orography larger than 750 m. The ECMWF (ERA40) precipitation forecasts at the dotted grid points are used to determine the area-mean and area-maximum precipitation representative for the south-western Alps.

Genoa cyclones. The yearly number of streamer days associated with heavy precipitation is reported also by Steinacker (MAP 2000) for the shorter period of 1989–98. He determined an averaged number of 3.3 days per year with a minimum of one and a maximum of nine streamer days. Similarly, Massacand *et al.* (1998) reported that about 2.5 events of moderate to heavy rain over southern Switzerland occur per year during the 1993–96 period.

In this note we apply another statistical approach in order to discuss the mutual evolution of the synoptic-scale streamer and of the regional-scale heavy rain on the Alpine southside. To this end the lagged regression method is used where atmospheric fields are regressed against time series of parameters or single-station time series with time lag τ to calculate lagged covariances (see von Storch and Zwiers (1999) for a brief introduction to this technique). Here the precipitation observed at the Alpine southside is chosen as a key parameter to study the associated co-development of synoptic-scale atmospheric fields in the Alpine region. We will combine analysed ERA40 meteorological fields with area-mean precipitation observed on the Alpine southside used also by MSZD. For reasons of comparison, additional statistics are determined based on ERA40 precipitation data forecast by the ECMWF model.

2. Data and Method

The daily averaged ERA40 analysis provided by the ECMWF is combined with daily area-averaged precipitation along the Alpine southside taken from the observed precipitation measures as in MSZD. Their data are taken from the daily high-resolution (25 km) gridded observational dataset provided by Frei and Schär (1998). From this a subset of 48 grid points is extracted and time series of area-averaged as well as area-maximum precipitation are determined, representing the 24-hour cumulative rain for the Swiss Alpine southside. Additionally we consider a subsample of days with extraordinary amounts of precipitation which are characteristic for PV-streamer-related heavy rain events. Following MZSD, the threshold value is taken to be 29 mm d^{-1} of area-mean rain on the Alpine southside. During the considered period 1966–99, 127 cases occurred, 56 of them were encountered during autumn.

In order to estimate the reliability of the ECMWF precipitation forecasts, the lagged regression method will be applied also using ERA40 forecasts for the following day. The area mean is determined by averaging over five grid points (Fig. 1). Clearly the ERA40 resolved Alpine orography is very smooth, not showing, for example, gaps and valleys, and the mean height of the main ridge is only about 1300 m.

It is well known from synoptic observations and also shown by the climatology of MSZD that the autumn is the peak season for the occurrence of streamers associated with heavy precipitation. The study of MSZD showed that during autumn there is a frequency of 51%, whereas the other seasons show much less abundance: 1%, 18% and 30% during winter, spring and summer, respectively. Due to this autumnal maximum we restrict ourselves to analyse only this season of the period from 1966 to 1999. In the following the precipitation time series are denominated by OP (observed), EP (ECMWF forecast, ERA40) and HP (daily observed rain rates exceeding 29 mm). Finally, the symbol $\overline{(\,)}$ denominates area-maximum values.

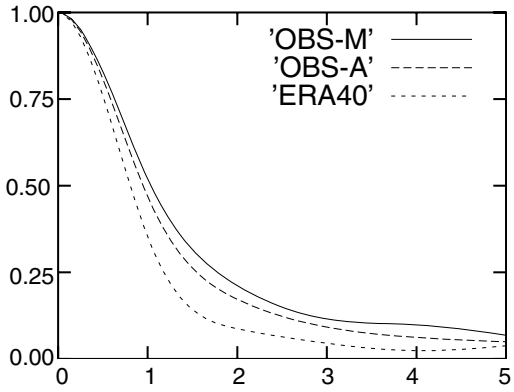

Figure 2. Auto-covariance of daily precipitation as a function of lag τ (days): observed area-maximum precipitation $\overline{\text{OP}}$ (OBS-M); observed area-mean OP (OBS-A); ERA40 precipitation EP (ERA40). The series contains all autumn days of 1966 to 1999.

3. CLIMATOLOGY

First we investigate the auto-correlation and cross-correlation properties of the individual precipitation time series. Figure 2 shows the auto-correlation of the time series: observed area-mean OP (OBS-A) and area-maximum $\overline{\text{OP}}$ (OBS-M) and EP (ERA40). The auto-covariance functions decay rapidly with lag, suggesting that strong precipitation events have a lifetime of 1 to 2 days. At longer lags, there is a tail with a slow decay. The observed area-maximum series shows the longest lifetime in comparison to all series, the shortest one results from the ERA40 series. Nevertheless, the differences between the time series are small.

In Table 1 various statistics of the precipitation time series are given. The cross-correlation coefficients are a measure of the quality of the relation of two data series, here observed and ERA40 precipitation. Clearly, all time series of precipitation have different intensities. The mean values averaged over the entire period 1966–99 are 3.6 (OP), 16.0 ($\overline{\text{OP}}$) and 1.2 (EP) mm d^{-1}; the latter value is about the same for the entire ERA40 period. The autumnally averaged values (SON) of the observed data are 3.8 (OP) and 17.2 ($\overline{\text{OP}}$) mm d^{-1}. The ERA40 series (EP) yields 1.2 mm d^{-1}, which is again the same value for the entire ERA40 period. The standard deviations σ are 0.8 (EP), 7.0 (OP), 29.8 ($\overline{\text{OP}}$) mm d^{-1}. These climatological statistics are completed by those determined for events with heavy precipitation HP. The mean value amounts to 35 mm d^{-1} and this value remains unchanged for autumn and the entire year. The corresponding σ are smaller than for the complete sample.

The correlation coefficient between the series EP and OP amounts to 0.69 for the period 1966 to 1999, and 0.70 for the autumnal subsample SON. The error for both coefficients is very small, partly because the data samples are quite large. Hence these correlation coefficients indicate a high degree of correspondence and underline the quality of the ERA40 precipitation data. The linear regression coefficient which describes the type of relation between both data series is around 0.25, again with a very small error.

Now we will discuss the cross-covariance fields of the individual precipitation time series with the atmospheric fields. Figure 3 shows the cross-covariance fields of observed mean precipitation OP, OP−HP and HP, with PV at potential temperature $\theta = 320$ K for lag $\tau = 0$. The fields are normalized by the standard deviation of the entire series in order to make the three fields comparable. The resulting fields can be interpreted in units of PV (1 pvu $= 10^{-6}$ K $\text{m}^2\text{kg}^{-1}\text{s}^{-1}$). Note the different isoline increments: 0.1 pvu (Figs. 3(a) and (b)) and 1.0 pvu (Fig. 3(c)). Obviously the strongest signal with more than 14 pvu appears with the HP events, whereas the climatological signal of non-HP events amounts to about 1 pvu. The climatological signal of the entire series (Fig 3(a)) appears at $\tau = 0$, with a maximum value of about 0.8 pvu. When the time series of the ERA40 precipitation is applied, the cross-covariance amplitudes increase by 0.1 pvu (not shown).

In Fig. 3(a), the determined cross-covariance function based on the OP sample shows a mixture of an elongated and circular pattern. For events with weak to moderate precipitation (non-HP events) the synoptic-scale pattern shows the cyclonic circular structure (Fig. 3(b)). The structure resulting from the HP sample (Fig. 3(c)) resembles, apparently, a meridionally elongated streamer pattern. This is corrobated by

TABLE 1. CORRELATION AND REGRESSION STATISTICS

		SON 1966–99	YEAR 1966–99	SON 1958–2001	YEAR 1958–2001
OP	N	3094	12 418	–	–
	average	3.8	3.6	–	–
	σ	7.0	6.0	–	–
HP	N	56	127	–	–
	average	35.0	35.0	–	–
	σ	5.0	4.7	–	–
OP − HP	N	3038	12 291	–	–
	average	3.2	3.2	–	–
	σ	5.5	5.1	–	–
$\overline{\text{OP}}$	N	3094	12 418	–	–
	average	17.2	16.0	–	–
	σ	29.8	23.5	–	–
EP	N	3094	12 418	4004	16 071
	average	1.2	1.2	1.2	1.1
	σ	0.8	2.5	0.8	2.1
OP versus EP	N	3094	12 418	–	–
	CC	0.70	0.69	–	–
	error	0.02	0.01	–	–
	RC	0.25	0.24	–	–
	error	0.01	0.01	–	–

N = sample size, σ = standard deviation, RC = regression coefficient, CC = correlation coefficient, SON = Sept–Nov.

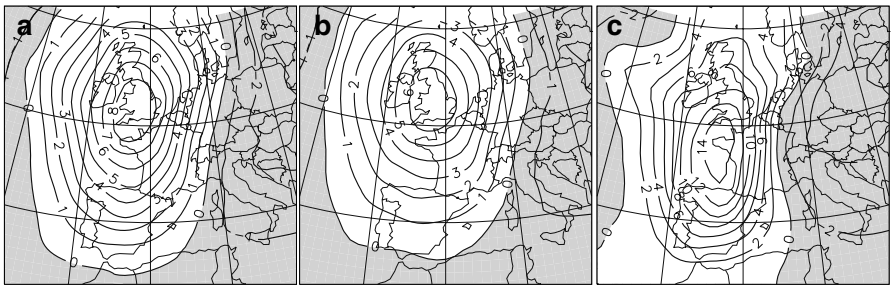

Figure 3. Cross-covariance function of precipitation with the PV field at potential temperature $\theta = 320$ K at $\tau = 0$, normalized by the corresponding standard deviation σ of the precipitation so that the resulting fields can be interpreted in units of pvu: (a) observed precipitation OP, (b) OP−HP, and (c) HP. The isolines are given in (a) and (b) 0.1 pvu, and (c) 1.0 pvu. The shaded area indicates negative cross-covariance function. The series covers all autumn days of 1966 to 1999.

the climatological study of MSZD where a similar meridional extent was determined. For days with weak precipitation they obtained a circular structure.

It is particularly noteworthy here that the zonal PV gradient (Fig. 3(c)) becomes strongest close to the Alps at $\tau = 0$ days. This is obvious from an indentation of the PV field above the western Alps. The corresponding regression fields (see Fig. 5) between $\tau = -1$ and $\tau = 0$ days show clearly that the pattern centre moves faster towards the Alps than the leading edge of the streamer. The pattern of maximum gradients above the western Alps indicates an apparent orographic impact on the streamer in retarding its leading edge above the Alps in comparison to regions north and south of the Alpine barrier. Also recent numerical simulations have shown that the streamer's PV is significantly reduced, particularly above the Alps as soon as the streamer crosses Central Europe (Morgenstern and Davies 1999; Hoinka *et al.* 2003).

Associated with the PV configuration is a corresponding cyclonic upper-level wind field, as can be gleaned from the cross-covariance horizontal wind fields at $\theta = 320$ K (Fig. 4). Figure 4(a) gives the result

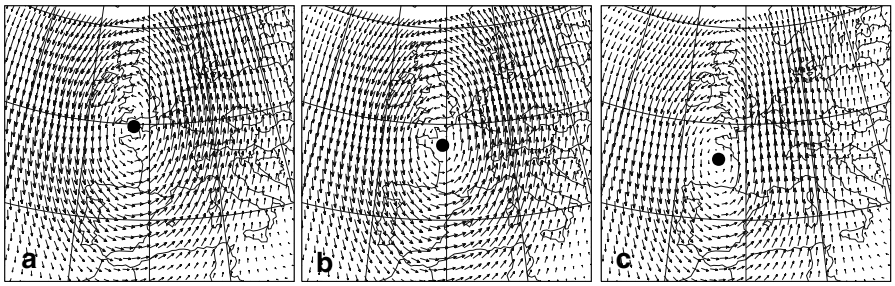

Figure 4. Cross-covariance function of precipitation with the wind field at potential temperature $\theta = 320$ K at $\tau = 0$, normalized by the corresponding standard deviation σ of the precipitation so that the resulting fields can be interpreted in units of m s^{-1}: (a) observed precipitation OP, (b) ERA40 precipitation EP, and (c) observed heavy precipitation HP. The maximum velocities are (a) 7.6, (b) 3.4 and (c) 149.6 m s^{-1}. The dots mark the low centres. The series covers all autumn days of 1966 to 1999.

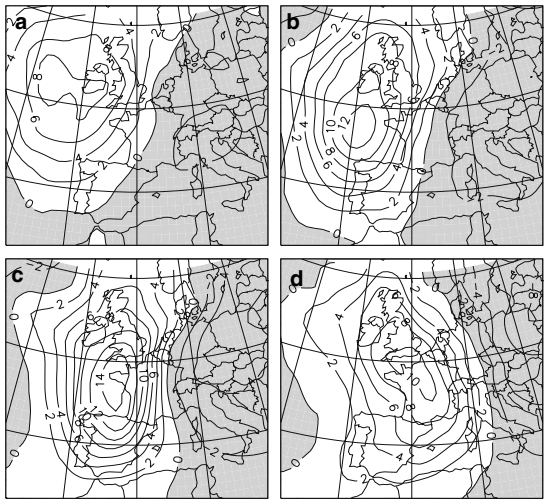

Figure 5. Cross-covariance functions of HP with the PV field at potential temperature $\theta = 320$ K normalized by the standard deviation σ of the precipitation so that the resulting fields can be interpreted in units of pvu. Time lags of (a) $\tau = -2$, (b) $\tau = -1$, (c) $\tau = 0$, and (d) $\tau = +1$ days. The isolines are given in 1.0 pvu. The shaded area indicates negative cross-covariance function. The series contains all autumn days of 1966 to 1999.

based on the observed precipitation series, whereas Fig. 4(b) is the result using the ERA40 precipitation. The slight difference is that the centres of the lows do not coincide. The statistical low centre resulting from the ERA40 forecasts is located about 2° further south as well as further east in comparison to the low centre obtained by applying the observed precipitation series. The HP events (Fig. 4(c)) exhibit a centre's location south of Brittany in France. The statistical low centre's location determined in the study of MSZD was located slightly further north, above Brittany.

Another notable feature is the strength and the zonal asymmetry in the regressed wind field across the streamer at $\tau = 0$. To the north of 43°N, about the latitude of northern Corsica, the magnitude of the northerly wind at the streamer's trailing edge is weaker than that of the southerly wind at its leading edge. Along the Alpine latitude there are remarkable differences between western minimum and eastern maximum in regressed meridional wind strength. For the HP sample the regressed maximum meridional component reaches -117 (west) and 149 (east) m s^{-1}, whereas the maximum zonal wind component north and south of the low's centre amounts to 73 and -64 m s^{-1}. The particularly strong southerly flow occurs in the area of 48°N and 5°E, approximately the north-western edge of the Alps. Selecting a sample of HP with a minor threshold value for the daily precipitation of 16.0 mm d^{-1}, the maximum wind speed at the leading edge of the streamer at 320 K decreases to 79 m s^{-1}. At 500 hPa the meridional wind

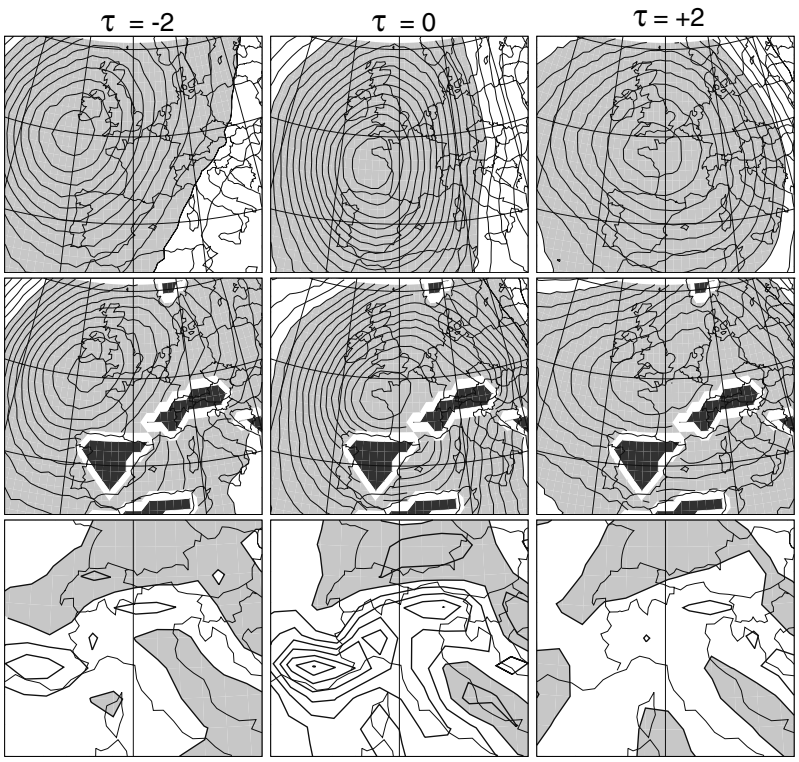

Figure 6. Cross-covariance function of HP with the pressure field at 5000 m (top row) and 500 m (centre row), and vertical velocity at 1500 m (bottom row). The fields are normalized by the standard deviation σ so that the resulting fields can be interpreted in units of hPa and mm s^{-1}, correspondingly. Isolines: 5.0 hPa and 5 cm s^{-1}; negative cross-covariances are shaded; there are no data within the black regions due to orography. Lags τ (days) as indicated. The series covers all autumn days of 1966 to 1999.

maximum at the leading edge results in 89 for HP, and in 50 m s^{-1} for the sample using the modified threshold. Morgenstern and Davies (1999) pointed out that the asymmetry can be linked to the reduced stratification and increased vorticity at the tropopause level that results from convective activity enhanced by orography. The asymmetry is also consistent with the injection of anomalously low-PV air into the upper levels occurring at the streamer's leading edge.

The lifetime of the heavy precipitation events (1–2 days; Fig. 2) determined from the auto-covariances forms the time window for our lagged regression analysis. Figure 5 shows cross-covariance fields of observed heavy precipitation HP with PV at $\theta = 320$ K for lags $\tau = -2$, -1, 0 and $+1$ days. Generally it is found that the amplitudes of regression patterns increase with τ towards zero and decrease for increasing positive lag. Figure 5 indicates meridional stretching and deepening of the PV regression pattern during the evolution towards $\tau = 0$. Noteworthy is also that during the approach towards and crossing above the Alps the meridional axis of the streamer turns anticlockwise.

The PV regression fields, given in Fig. 5 suggest an influence of the Alps on the mid- to upper-tropospheric leading edge of the streamer. At the surface the orographic impact is clearly apparent in the cross-covariance function of the precipitation HP with the pressure field at 500 m height (Fig. 6, centre row), and is strongest at $\tau = 0$. However, up to a height of 5000 m the orographic signal vanishes (Fig. 6, top row). The orographically enhanced vertical velocity, here at 1500 m, is also strongest at $\tau = 0$ (Fig. 6, bottom row). Two separate maxima appear, one above the south-western Alps and another in north-eastern Italy. Up to three days (not shown) in advance of the peak time of the precipitation event, there is an area with significant vertical velocity south of the western Alps which is also clearly due to streamer-related southerly low-level flow. After $\tau = 0$ the vertical velocity signal vanishes rapidly.

The southerly flow of moist air towards the Alps is demonstrated statistically for HP in Fig. 7, where the top and centre rows show the regression fields of meridional humidity flux. At 1500 m (Fig. 7, centre)

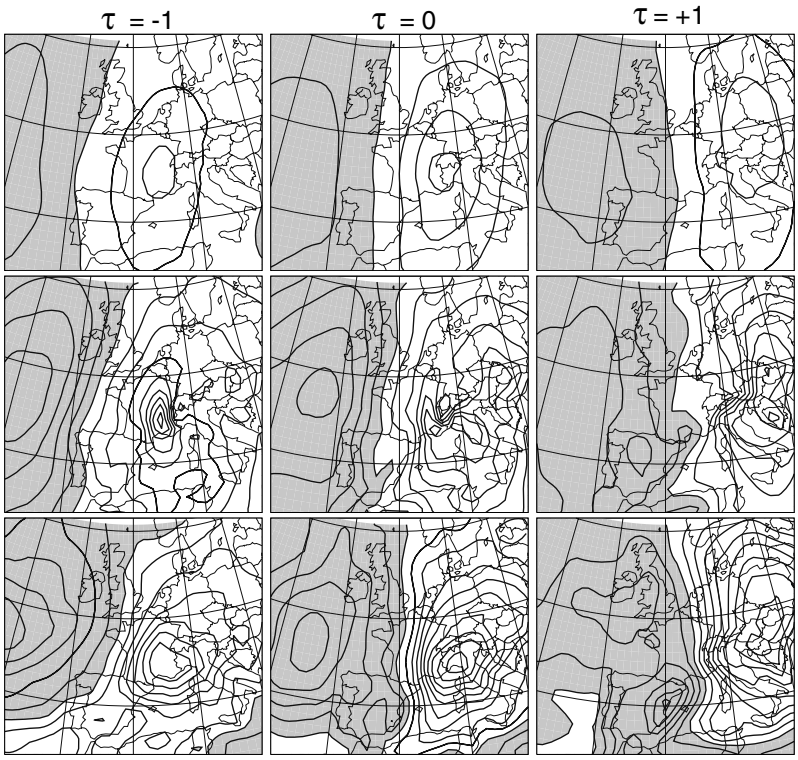

Figure 7. Cross-covariance function of HP with the humidity flux fields at 5000 m (top row) and 1500 m (centre row), and vertically integrated humidity at the lowest 3000 m (bottom row). The humidity fields are normalized by the standard deviation σ so that the resulting fields can be interpreted in units of g kg^{-1}m s^{-1} and g kg^{-1}, correspondingly. Isolines: 50 g kg^{-1}m s^{-1} and 1 g kg^{-1}; negative cross-covariances are shaded. Lags τ (days) as indicated. The series covers all autumn days of 1966 to 1999.

the main flux occurs along the western side of the Alps at $\tau = -1$ day, followed by a strong southerly flux towards the entire Alps at $\tau = 0$ and a weaker one over the Balkans at $\tau = +1$ day. The mid-tropospheric flux pattern at 5000 m (Fig. 7, top row) shows a balanced distribution, west/east of the streamer's axis, up to $\tau = -1$ day. However, at $\tau = 0$ appears a clear signal of stronger humidity fluxes along the eastern part of the streamer. The vertical integral of humidity between the surface and 3000 m (Fig. 7, bottom row) exhibits a significant maximum above northern Italy at $\tau = 0$.

Finally maximum values of various regressed parameters are summarized in order to illustrate the remarkable difference between the climatic state (OP) and heavy precipitation events (HP) at $\tau = 0$. The PV signal is 0.8 (14) pvu for OP (HP); the southerly flow at the leading edge at 320 K results to 7 (149) m s^{-1}; the regressed vertical velocity on the Alpine southside reaches 10 (300) mm; the vertically integrated humidity over the lowest 3000 m amounts to 0.5 (9.0) g kg^{-1}; the northerly humidity flux at 1500 m above the southern Alps is 12 (300) g kg^{-1}m s^{-1}.

4. Summary and conclusions

In this note we discussed lagged regression of ERA40 atmospheric fields with time series of observed and predicted precipitation. In spite of the apparent differences in intensity between *in situ* observed precipitation and ECMWF forecasts, the results of the lagged regression using both series show a similar behaviour (cf. Fig. 2). This points to the fact that the ECMWF precipitation forecast seems to capture, reasonably well at least, the evolution of heavy precipitation but obviously not the intensity. One reason for this is that the orographic representation is not sufficient. Moreover, Fig. 2 suggests that events with observed heavy precipitation have a slightly longer period in duration than indicated by simulated precipitation from ERA40.

The regression analysis yields a pattern with the typical geographical position of the PV-streamer when flooding occurs at the southern side of the Alps: quasi-north–south aligned; extending southward over the Mediterranean Sea with its southern end located between the Pyrenees and northern Africa. The statistical results of lagged regressions indicate that the zonal PV gradient across the streamer's leading edge becomes strongest close to the Alps with τ increasing towards zero. We find an indentation in PV above the western Alps which is strongest during $\tau = -1$ and $\tau = +1$ days, indicating an apparent orographic impact on the streamer. Noteworthy is also that during the approach toward and crossing above the Alps the meridional axis of the streamer turns anticlockwise.

The regressed upper-tropospheric horizontal winds are strong in heavy precipitation cases, particularly at the streamer's leading edge where the meridional winds have their maximum at the north-western edge of the Alps. The regressed lower-tropospheric vertical wind field is strongest at $\tau = 0$ above northern Italy, exhibiting two separate maxima, one at the western and another above the eastern Alps. Prior to the heavy precipitation maximum significant vertical velocity is determined south of the western Alps.

The meridional low-tropospheric humidity flux is strongest towards the entire Alpine ridge at $\tau = 0$. At $\tau = -1$ days, i.e. one day earlier, a strong southerly flux is determined west of the French Alps. There exists an apparent asymmetry between the western and eastern part of the streamer in the vertically integrated humidity content beneath 5000 m showing much more humidity at the eastern part, possibly reflecting the moisture advection from the warm and moist Mediterranean Sea as opposed to the drier flow from the north.

Forecasting precipitation is one of the most critical and challenging tasks for an operational forecaster. Empirical forecast aids, such as the relationship between jet stream position and moisture-laden regions (e.g. Smith an Younkin 1972), do have some merits. In a similar way, the climatological statistics presented here can be useful, because they describe those synoptic-scale patterns which precede and co-exist with high probability in dangerous situations when heavy precipitation occurs with eventually local flooding. This might help forecasters as a first aid to put themselves into a state of alert.

References

Appenzeller, C. and Davies, H. C. 1992 Structure of stratospheric intrusions into the troposphere. *Nature*, **358,** 570–572

Bougeault, P., Houze, R. A., Rotunno, R. and Volkert, H. (Eds.) 2003 Special issue of MAP. *Q. J. R. Meteorol. Soc.*, **129,** 341–899

Frei, C. and Schär, C. 1998 A precipitation climatology of the Alps from high-resolution rain-gauge observations. *Int. J. Clim.*, **18,** 873–900

Hoinka, K. P., Richard, E., Poberaj, G., Busen, R., Caccia, J. L., Fix, A. and Mannstein, H. 2003 Analysis of a potential-vorticity streamer crossing the Alps during MAP IOP-15 on November 1999. *Q. J. R. Meteorol. Soc.*, **129,** 609–632

Holopainen, E. O. and Rontu, L. 1981 On shear lines in the upper troposphere over Europe. *Tellus*, **33,** 351–359

MAP 2000 'A successful field phase'. US MAP Project Office, February 2000. Boulder CO, USA

Martius, O., Zenklusen, E., Schwierz, C. and Davies, H. C. 2006 Episodes of Alpine heavy precipitation with an overlying elongated stratospheric intrusion: A climatology. *Int. J. Clim.*, **26,** 1149–1164, doi: 10.1002/joc.1295

Massacand, A. C, Wernli, H. and Davies, H. C. 1998 Heavy precipitation on the Alpine southside: An upper-level precursor. *Geophys. Res. Lett.*, **25,** 1435–1438

Morgenstern, O. and Davies, H. C. 1999 Disruption of an upper-level PV-streamer by orography and cloud-diabatic effects. *Contr. Atmos. Phys.*, **72,** 173–186

Simmons, A. J. and Gibson, J. K. 2000 'The ERA-40 Project Plan'. ERA-40 Project Report Series No. 1. European Centre for Medium-Range Weather Forecasts, Shinfield Park, Reading, Berkshire RG2 9AX, UK

Smith, W. and Younkin, R. J. 1972 An operationally useful relationship between the polar jet stream and heavy precipitation. *Mon. Weather Rev.*, **100,** 434–440

von Storch, H. and Zwiers, F. W. 1999 *Statistical analysis in climate research.* Cambridge University Press

Volkert, H. (Ed.) 2000 Heavy precipitation in the Alpine region (HERA). *Meteorol. Atmos. Phys.*, **72,** 71–270